energies

MDPI

Article

The Effect of Initial Conditions on the Laminar Burning Characteristics of Natural Gas Diluted by CO_2

Zhiqiang Han [1], Zhennan Zhu [2,*], Peng Wang [1], Kun Liang [2], Zinong Zuo [1] and Dongjian Zeng [1]

[1] Key Laboratory of Fluid and Power Machinery, Ministry of Education, Xihua University, Chengdu 610039, China
[2] Department of Engineering and Design, University of Sussex, Brighton BN1 9QT, UK
* Correspondence: zhennan.zhusussex@outlook.com; Tel.: +86-183-8046-0192

Received: 17 May 2019; Accepted: 17 July 2019; Published: 27 July 2019

Abstract: The initial conditions such as temperature, pressure and dilution rate can have an effect on the laminar burning velocity of natural gas. It is acknowledged that there is an equivalent effect on the laminar burning velocity between any two initial conditions. The effects of initial temperatures (323 K–423 K), initial pressures (0.1 MPa–0.3 MPa) and dilution rate (0–16%, CO_2 as diluent gas) on the laminar burning velocity and the flame instability were investigated at a series of equivalence ratios (0.7–1.2) in a constant volume chamber. A chemical kinetic simulation was also conducted to calculate the laminar burning velocity and essential radicals' concentrations under the same initial conditions. The results show that the laminar burning velocity of natural gas increases with initial temperature but decreases with initial pressure and dilution rate. The maximum concentrations of H, O and OH increase with initial temperature but decrease with initial pressure and dilution rate. Laminar burning velocity is highly correlated with the sum of the maximum concentration of H and OH.

Keywords: natural gas; diluent gas; laminar burning velocity; flame instability; concentration of radicals

1. Introduction

Natural gas, of which the major constituent is methane, is now regarded as a promising alternative fuel with excellent prospects owing to its huge quantity, cleaner emissions and high thermal efficiency [1–3]. In order to reduce the emissions and to improve engine performance, combining hydrogen-natural gas blending fuel with exhaust gas recirculation (EGR) [4–8] is a feasible approach. However, the addition of EGR has a certain impact on combustion. Many researchers have conducted research on the combustion characteristics of natural gas [9–12].

To date, laminar flame and chemical kinetic models of natural gas is increasingly interesting to many researchers. Zeng [13] investigated the ignition characteristics of methane-air mixture. Their results showed that GRI mech_3.0 mechanism gave the most accurate prediction on ignition delay time comparing to USC_2.0 mechanism and NUI_Galway mechanism, and the ignition delays were sensitive to small radicals such as H, O and OH. However the burning velocity was not taken into account. Xu [14] investigated the chemical effect of CO_2 on laminar flame speed of CH_4. The conclusion that the chemical effect was stronger than radiative effect but weaker than thermal effect was confirmed, but the flame instability was not investigated.

Many researchers have also studied the effects of initial conditions on the combustion characteristics of flames. Zhang et al. [15] analyzed the influence on the laminar burning velocity and Markstein length. The results show that the laminar burning velocity of dissociated methanol-air mixture increases with

an increase in initial temperature and decreases with an increase in initial pressure. The Markstein length decreases with an increase in initial temperature and initial pressure. By using a constant volume chamber, Miao et al. [16] studied the influence of fuel-air equivalent ratio, hydrogen-doping ratio and dilution degree on the laminar burning velocity and Markstein length for the hydrogen-mixed natural gas-air-diluted gas. The results show that the laminar burning velocity decreases when the hydrogen doping ratio decreases and the dilution increases. The diluent gas CO_2 inhibits the laminar burning velocity more than N_2. The diluent is an inert gas that hardly participates in the chemical reaction, but has the dual functions of dilution and heat absorption. Therefore, the addition of diluent gas slows down the chemical reaction rate of the mixture, resulting in a decrease in flame propagation speed and burning velocity; The increase of the initial temperature of the constant volume chamber will promote the chemical reaction rate of the mixed gas, while the increase of the initial pressure will inhibit the chemical reaction rate of the mixed gas. Therefore, there should be an equivalent effect between the dilution rate, the initial temperature and the initial pressure on the laminar burning velocity of the mixed gas. In this paper, the effect of initial conditions (initial temperature, initial pressure, dilution ratio and equivalence ratio) on burning characteristics (laminar burning velocity, flame instability, flame structure and concentration of essential radicals) are investigated comprehensively.

2. Experimental Setup

The experiments in this study were conducted in a constant volume chamber (CVC) test system with wrapped in heating tapes and surrounded by thermo-insulating asbestos, which can heat the bomb to the set initial temperature and reduce the heat loss as well. The test rig is capable of temperature monitoring and controlling, data acquisition, Schlieren photographing, ignition, intake and exhaust. The temperature was measured by a type-K thermocouple and controlled by a proportional-integral-derivative (PID) controller within ±3 K. The data acquisition system includes a pressure sensor (type 6125C, KISTLER, Winterthur, Switzerland), a data acquisition card (DAQ, type USB-6365, sampling frequency 100 KHz, NI, Austin, TX, USA) and a charge amplifier (type 5018A, KISTLER). The Schlieren system consists of an illuminant (power 100 W), two concave reflecting mirrors (focal length 110 mm), two plane reflecting mirrors and a high speed digital camera (type V7.3, frequency 10,000 fps, image resolution 512 × 512 pixels, Phantom, Wayne, IN, USA). Ignition, photographing and data acquisition were triggered simultaneously by a controller (type Calibration V2, ECTEK, Changzhou, China).

Table 1 shows parameters of the constant volume chamber. Figure 1 shows the CVC experimental setup. The CVC was evacuated initially, and each gas can then be charged to the specified pressure in the order of CO_2, natural gas and compressed air, and the mixture was heated to the initial temperature; Before ignition, the mixture was premixed for at least 5 min; After combustion, the valve and air compressor were opened to discharge the residual exhaust gas, and then the CVC was cleaned by fresh air three times to ensure that there was no residual exhaust gas influence for the following test.

Table 1. Parameters of the constant volume chamber.

Parameter (Unit)	Value
Inner diameter (mm)	350
Volume (L)	22.4
Maximun heating temperature (K)	600
Maximum pressure (MPa)	4
Effective diameter of windows (mm)	Φ120
Primary ignition voltage (V)	14
Ignition electrode gap (mm)	2
Ignition pulse width (ms)	2

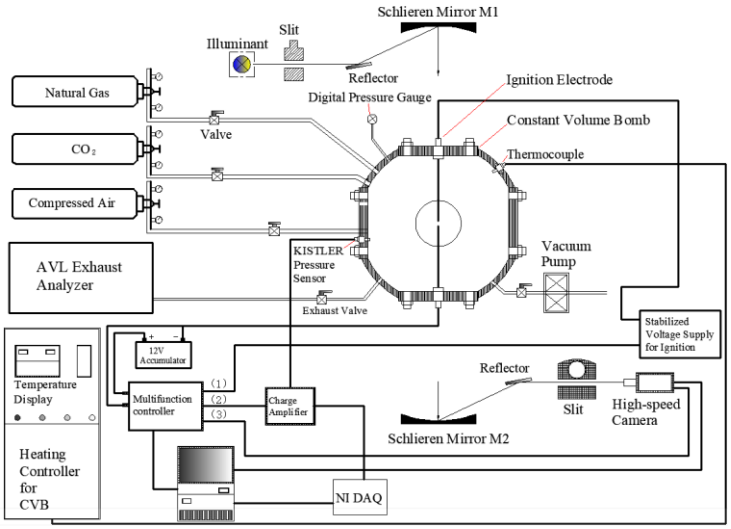

Figure 1. The experimental setup, consisting of a constant volume chamber, a Schlieren system, a temperature controlling and monitoring system, an intake and exhaust system, an AVL exhaust analyzer and a computer as a controller.

In order to avoid the influence of ignition energy and combustion pressure change on the combustion analysis [17], the laminar combustion characteristics were analyzed mainly in the flame radius of 6 mm to 25 mm.

In this study, dilution rate (*DR*) is defined as the mole fraction of CO_2 in mixtures, which is calculated according to Equation (1). Table 2 lists the test conditions of natural gas-CO_2-air blending fuel. Natural gas used in this study is mainly composed of methane:

$$DR = V_{CO_2} / (V_{CH_4} + V_{CO_2} + V_{air}) \quad (1)$$

Table 2. Test conditions of natural gas-CO_2 mixture.

Parameter (Unit)	Value
Initial temperature T_u (K)	323, 348, 373, 398, 423
Initial pressure p_u (MPa)	0.1, 0.15, 0.2, 0.25, 0.3
Φ	0.7, 0.8, 0.9, 1.0, 1.1, 1.2
DR (%)	0, 2, 4, 6, 8, 10, 12, 14, 16

3. Data Processing

3.1. Extraction of Flame Radius

The Schlieren photographs were analysed to compute the flame radius. In this study, canny edge detector was applied to detect the boundary of the photograph due to its high accuracy, and there were five steps before detecting the boundary, named background removed, gray-scale contrast enhanced, extracted flame front, boundary identified and fitting, respectively. Three diameters (6 radii) were extracted with the interval angle of 60° (the horizontal line was regarded as X axis, and the positive side was regarded as 0° while the negative side was regarded as 180°). The average of these 6 values was computed, which is regarded as the radius of a photograph. These were implemented in MATLAB (type R2016a, The MathWorks, Natick, MA, USA). The diagram of extracting the flame radius is shown in Figure 2.

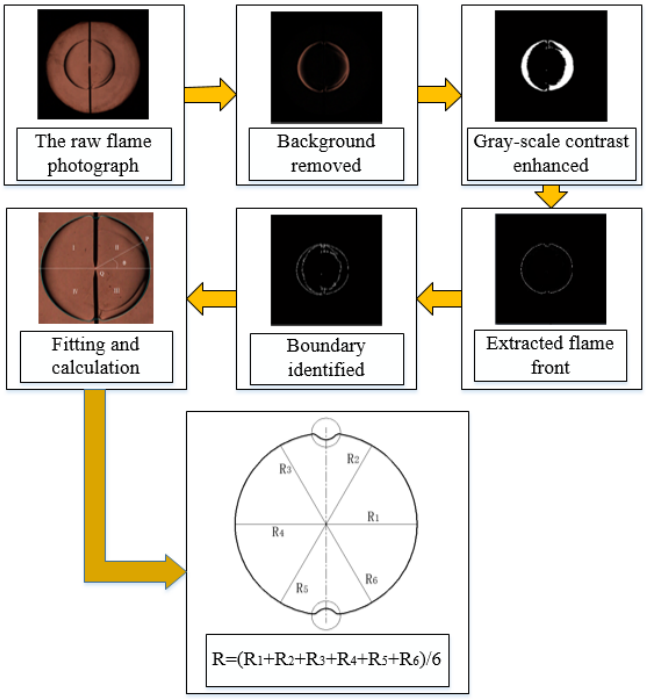

Figure 2. Diagram of extracting the flame radius.

3.2. Data Calculation

The instantaneous stretched flame propagation speed can be calculated as instantaneous radius versus time, as shown below:

$$S_n = \mathrm{d}R_\mathrm{u}/\mathrm{d}t \tag{2}$$

The stretch rate can be calculated as logarithm of a tiny area on spherical flame surface versus time, shown as follows:

$$K = \mathrm{d}(\ln A)/\mathrm{d}t = 2S_\mathrm{n}/R_\mathrm{u} = \kappa S_\mathrm{n} \tag{3}$$

In which $\kappa = 2/R_\mathrm{u}$ is the curvature of the flame front.

To obtain the un-stretched flame propagation speed and Markstein length, there are three models named linear model, non-linear model I and non-linear model II respectively, shown in Equations (4) and (5) [18] and Equation (6) [19]:

$$S_\mathrm{l} - S_\mathrm{n} = L_\mathrm{b}K \tag{4}$$

$$S_\mathrm{n} = S_\mathrm{l} - S_\mathrm{l}L_\mathrm{b}\kappa \tag{5}$$

$$\ln(S_\mathrm{n}) = \ln(S_\mathrm{l}) - S_\mathrm{l}L_\mathrm{b}\kappa/S_\mathrm{n} \tag{6}$$

According to Chen [20] the selection of model is based on Lewis number, which is defined as ratio of thermal diffusion to mass diffusion (methane to nitrogen when $\Phi < 1.0$, oxygen to nitrogen when $\Phi > 1.0$):

$$Le = \lambda/\rho_\mathrm{u}c_\mathrm{p}D_\mathrm{m} = D_\mathrm{T}/D_\mathrm{m} \tag{7}$$

where λ is the thermal conductivity, ρ_u is density of unburned gas, c_p is specific heat at constant pressure of the mixture. Non-linear model I is the most suitable model for mixtures whose $Le > 1$ while non-linear model II is the most suitable model for mixtures whose $Le < 1$.

The unstretched laminar burning velocity can be calculated as below:

$$u_\mathrm{L} = S_\mathrm{l}(\rho_\mathrm{b}/\rho_\mathrm{u}) = S_\mathrm{l}/\sigma \tag{8}$$

where σ is density of burned gas, σ is thermal expansion ratio. In this study, σ was calculated from initial physical parameters while σ was computed by a thermal equilibrium model in Chemkin-Pro.

The flame thickness can be calculated through Equation (9):

$$l_f = \lambda / \rho_u u_L c_p \tag{9}$$

3.3. Uncertainty in Schlieren Method

According to Zuo [21], the uncertainty mainly comes from the error in Schlieren photograph analysis, model selection, the calculation error sensitive to stretch rate and the inaccuracy caused by ignition and radiation.

In this study, the maximum error in photograph recognition is 1 pixel, leading to a maximum error in radius of 0.25 mm. The minimum interval among the photographs is 0.2 ms, resulting in a maximum stretched flame propagation speed of 1.25 m·s^{-1}, and thus a maximum error in laminar burning velocity of approximately 0.01 m·s^{-1}. The uncertainty due to model selection and ignition is negligible as the most suitable model and photographs with suitable radii were selected.

According to Cai [22], the uncertainty caused by radiation can be calculated by Equation (10):

$$u_{L,RCFS} - u_{L,EXP} = 0.82 u_{L,EXP} (u_{L,EXP}/S_0)^{-1.14} (T_u/T_0)(p_u/p_0)^{-0.3} \tag{10}$$

where $u_{L,EXP}$ is the experimentally measured laminar burning velocity while $u_{L,RCFS}$ is the laminar burning velocity with radiation taken into account. There are three constants in this equation, S_0 = 0.01 m·s^{-1}, T_0 = 298 K, p_0 = 0.1 MPa. The maximum uncertainty resulting from radiation in this study was approximately 0.006 m·s^{-1} (negligible).

Lowry [23] proposed a formula to calculate the inaccuracy in flame speed:

$$\delta_{S_l} = \sqrt{(B_{S_l})^2 + \left(t_{M-1.95} S_{S_l} / \sqrt{M}\right)^2} \tag{11}$$

where δ_{S_l} is the total bias uncertainty, which can be calculated as Equation (11) [23]. B_{S_l} is the system error, $t_{M-1.95}$ is t value at a 95% confidence interval and $M - 1$ degrees of freedom, S_{S_l} is the standard deviation of repeated experiments, and M is the number of repeated experiments per test point. It is clear that the more the repeated experiments are, the smaller the uncertainty is:

$$B_{S_l} = \sqrt{\sum_{i=1}^{n} \{u_i [\partial S_l(x_i)/\partial x_i]\}^2} \tag{12}$$

where u_i is the fixed error for each variable x_i, $S_l(x_i)$ describes the relationship between the flame speed and each variable x_i. According to Lowry [23], for test points with fixed initial temperature and pressure, $S_l(x_i)$ is just a function of equivalence ratio:

$$S_{l,u} = (a + b\phi + c\phi^2) \times (1/p_i)^{(d + e\phi + f\phi^2)} \tag{13}$$

For methane, the values are shown in Table 3. In this study, equivalence has a tolerance of ±(0.03–0.05), resulting in an error in laminar burning velocity of ±(0.008–0.011) m·s^{-1}. Each test point was conducted for three times to reach a higher accuracy.

Table 3. Correlation Coefficients for Methane.

A	B	C	D	E	F
−141.362	331.485	−156.243	2.586	−4.390	2.174

3.4. Chemical Kinetic Model

GRI_mech 3.0 was adopted in the simulation study by using Chemkin Pro. GRI_mech is a series of mechanisms aiming for combustion of methane, which were proposed by Gas Research Institute, and GRI_mech 3.0 is the latest version [24]. GRI_mech 3.0 mechanism contains 53 components and 325 elementary reactions and works well in combustion of methane, carbon monoxide, hydrogen, etc.

4. Results and Discussion

4.1. Laminar Burning Velocity

In this study, laminar burning velocities were calculated from both Schlieren images (see as Appendix A) and Chemkin model, and the results from these two methods show small differences. The validation of experimental experimental study is conducted by comparing present data with previous data [22,25], and the simulation model is validated by comparing them with experimental data, as shown in Figure 3. It is clear that laminar burning velocities from Schlieren and Chemkin agree well. The present results are close to literature results. Error bars in burning velocity from Schlieren are shown in corresponding graphs.

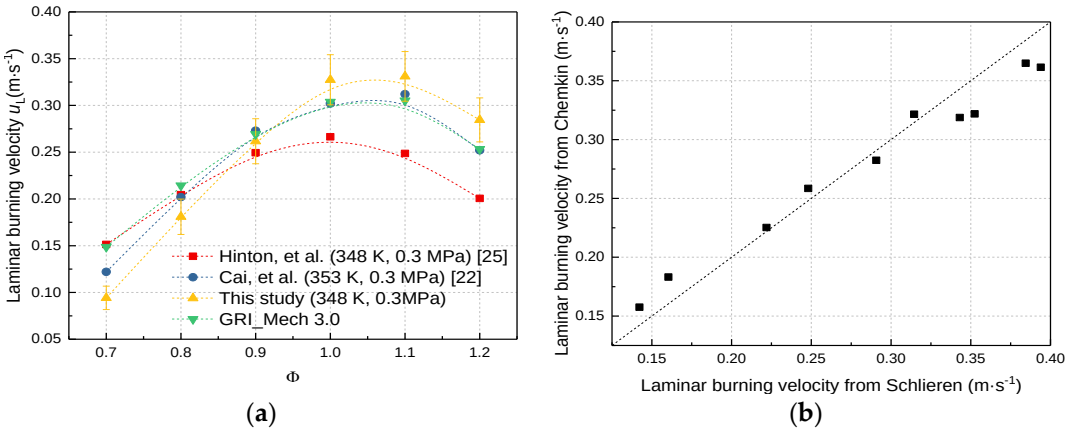

Figure 3. Validation of present experimental and simulation studies. (**a**) Comparing with previous data; (**b**) Comparing Chemkin with Schlieren.

Figure 4 shows the laminar burning velocities under different initial temperatures (initial pressure of 0.2 MPa, dilution rate of 0%). It is clear that the laminar burning velocity increases to a peak value and then decreases with increased equivalence ratio. The peak burning velocity occurs at equivalence ratio of 1.0–1.1, and it does not change with varying initial temperature, which agrees with what was reported in previous study [15]. On both the lean and rich sides, laminar burning velocities under higher initial temperature are larger than those under lower initial temperature. It can be concluded that elevating initial temperature will result in an extended flammable limit.

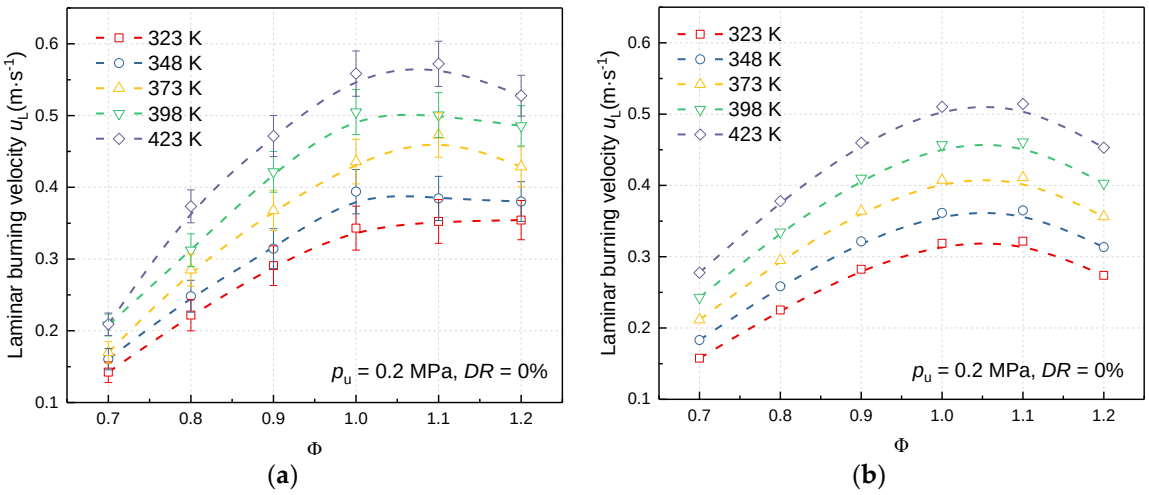

Figure 4. Laminar burning velocities under different initial temperatures (initial pressure of 0.2 MPa, dilution rate of 0%). (**a**) From Schlieren; (**b**) From Chemkin.

Figure 5 shows the laminar burning velocities under different initial pressures (initial temperature of 423 K, dilution rate of 0%). At both lean and rich sides, laminar burning velocities under lower initial pressure are larger than those under higher initial pressure. Under each initial pressure, the peak burning velocity occurs at equivalence ratio of 1.0–1.1 and does not shift when initial pressure changes.

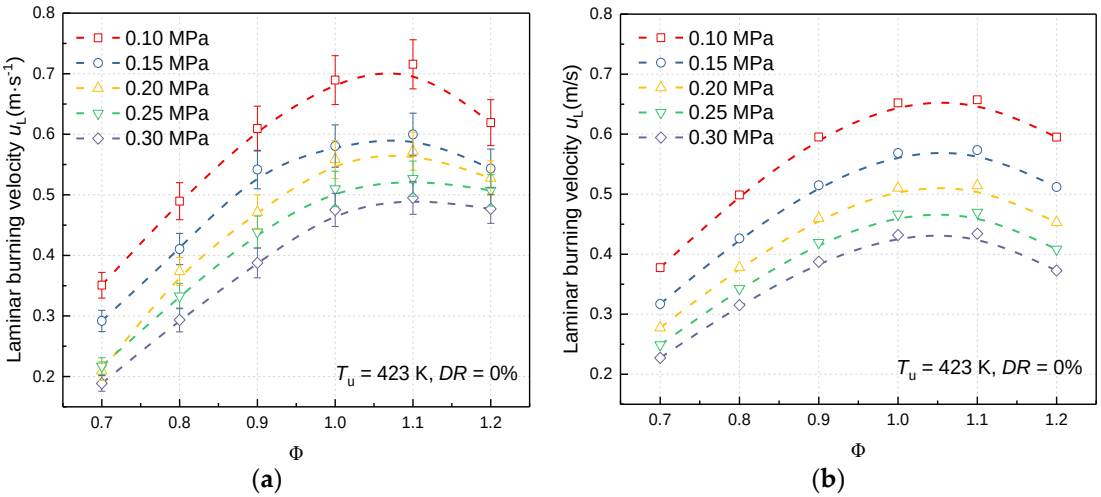

Figure 5. Laminar burning velocities under different initial pressures (initial temperature of 423 K, dilution rate of 0%). (**a**) From Schlieren; (**b**) From Chemkin.

Figure 6 shows the laminar burning velocities under different dilution rates (initial temperature of 423 K, initial pressure of 0.1 MPa). At both lean side and rich side, laminar burning velocities under lower dilution rate are larger than those under higher dilution rate. Decreasing dilution rate will result in an extended flammable limit. The peak burning velocity occurs at equivalence ratio of 1.0–1.1, but it shift towards stoichiometric mixture slightly with an increasing fraction of CO_2.

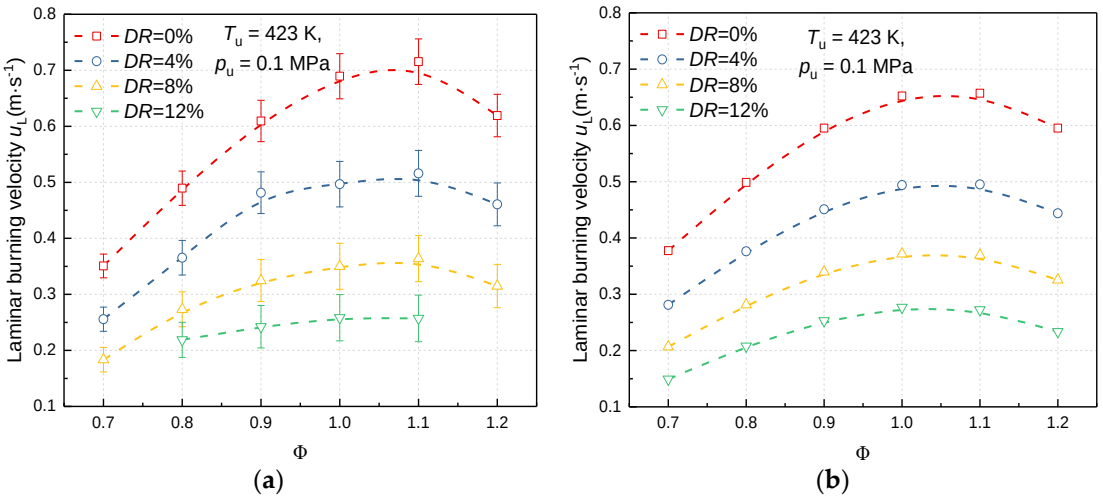

Figure 6. Laminar burning velocities under different dilution rates (initial temperature of 423 K, initial pressure of 0.1 MPa). (**a**) From Schlieren; (**b**) From Chemkin.

From Figure 4b, the intervals among each curve are very close. For the stoichiometric mixture, the interval values are 0.043 m·s^{-1}, 0.046 m·s^{-1}, 0.050 m·s^{-1} and 0.053 m·s^{-1} respectively. From Figure 5b, the intervals among curves show an increasing trend with decreasing initial pressure. For stoichiometric mixture, the interval values are 0.035 m·s^{-1}, 0.044 m·s^{-1}, 0.058 m·s^{-1} and 0.084 m·s^{-1} respectively. From Figure 6b, the intervals among curves show an increasing trend with decreasing fraction of CO_2. For stoichiometric mixture, the interval values are 0.095 m·s^{-1}, 0.122 m·s^{-1} and 0.158 m·s^{-1},

respectively. Figure 7 illustrates the interval values at stoichiometric ratio, with linear fitting applied. The R-Square is a value to evaluate the linearity. The closer it gets to 1, the higher the linearity is. It is clear that the intervals in burning velocity among different temperature have the highest linearity.

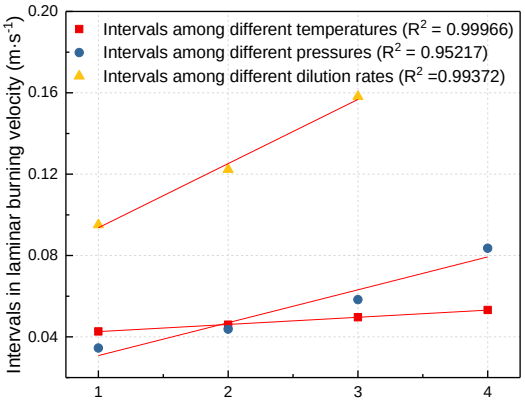

Figure 7. Fitting of the interval values.

4.2. Flame Structure and Concentration of Radicals

4.2.1. Flame Structure

Flame structure mainly shows the mole fraction of reactants (CH_4 and O_2), products (CO, H_2, CO_2 and H_2O) and radicals (OH, H, O, HO_2 and H_2O_2) versus the distance from the burner. Figures 8–10 illustrate the flame structures under different initial pressures, initial temperature and dilution rates, respectively. It can be seen that the mole fractions of reactants and products are of the largest order, from 10^{-2} to 10^{-1}. For the radicals, OH, H and O are of the order of 10^{-3}. Among these three kinds of radicals, OH accounts for the largest fraction, followed by H, and the fraction of O is the smallest. HO_2 and H_2O_2 are of the order of 10^{-4} and HO_2 is more than H_2O_2. The results can agree well with [24].

From Figure 8, fractions of reactants and products are approximately constant after the reaction under each initial pressure. When the distance is between 0.1 cm and 0.2 cm, the curves of reactants and products' fractions are steeper, which means that the concentration of each reactant or product in the main reaction zone is more sensitive to the distance. It may be speculated that increasing initial pressure can reduce the size of reaction zone. For the radicals, fractions of HO_2 and H_2O_2 just rise slightly with an increasing in initial pressure while there are significant increases in fractions of OH, H and O. So it can be concluded that concentrations of OH, H and O mainly influence the combustion process, which agrees with previous research [26].

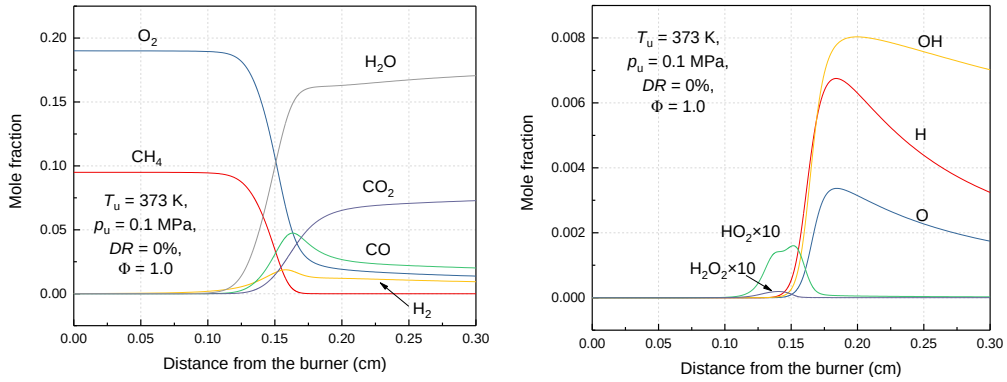

(a)

Figure 8. *Cont.*

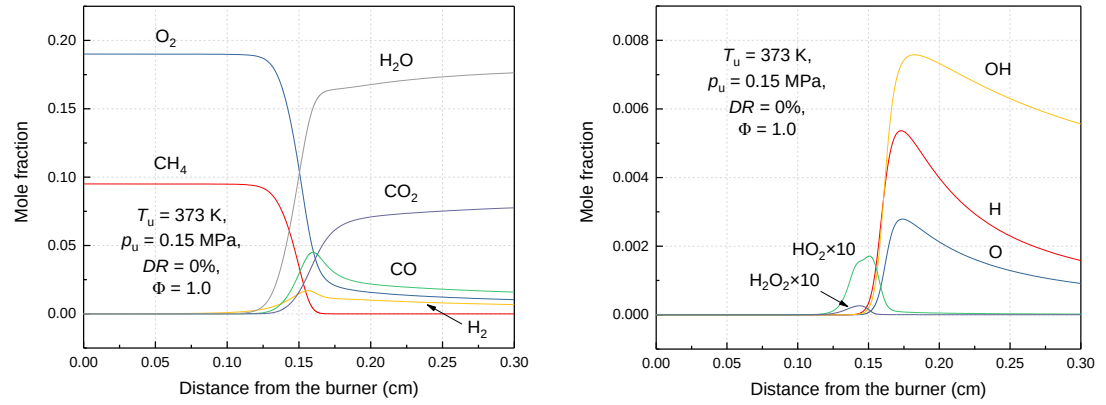

(**b**)

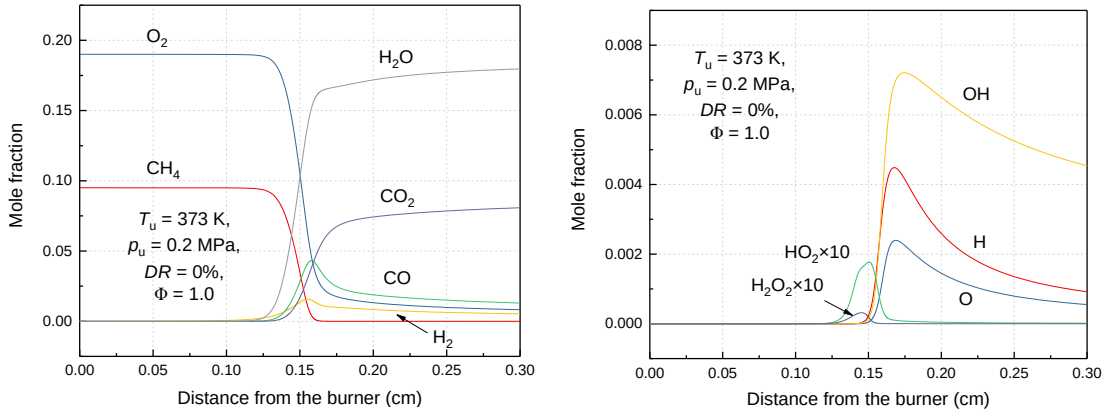

(**c**)

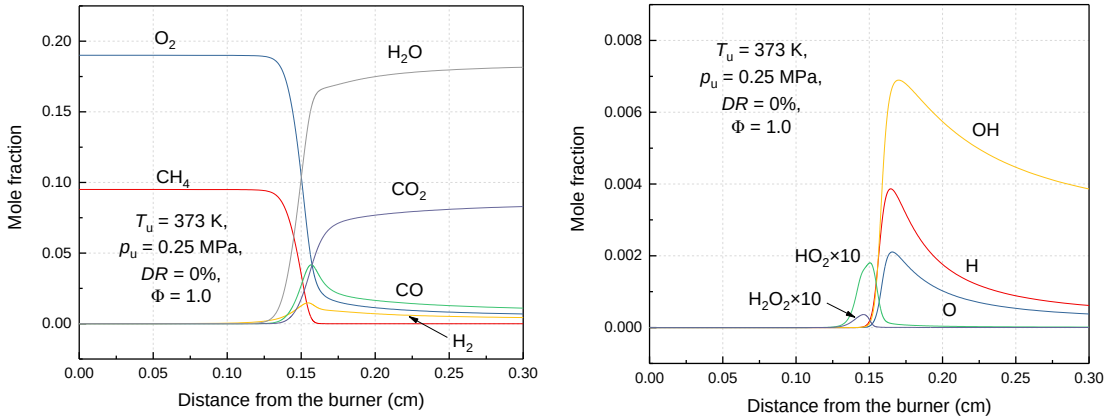

(**d**)

Figure 8. *Cont*.

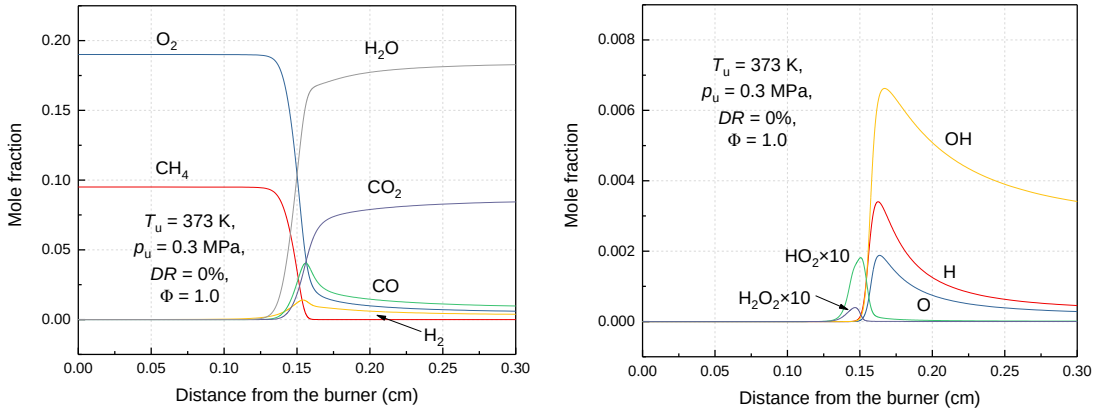

(**e**)

Figure 8. Flame structures under different initial pressures. (**a**) T_u = 373 K, p_u = 0.1 MPa, *DR* = 0%, Φ = 1.0; (**b**) T_u = 373 K, p_u = 0.15 MPa, *DR* = 0%, Φ = 1.0; (**c**) T_u = 373 K, p_u = 0.2 MPa, *DR* = 0%, Φ = 1.0; (**d**) T_u = 373 K, p_u = 0.25 MPa, *DR* = 0%, Φ = 1.0; (**e**) T_u = 373 K, p_u = 0.3 MPa, *DR* = 0%, Φ = 1.0.

From Figure 9, initial and final concentrations of reactants and products do not have significant variations. For the radicals, with initial temperature increasing, fractions of HO_2 and H_2O_2 almost stay constant while fractions of OH, H and O rise obviously. This can also confirm the close relation between OH, H, O and laminar burning velocity.

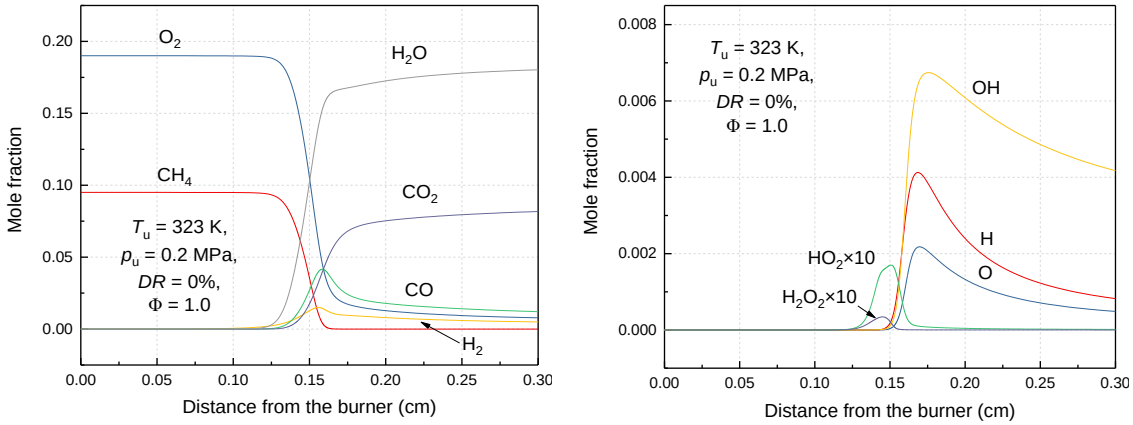

(**a**)

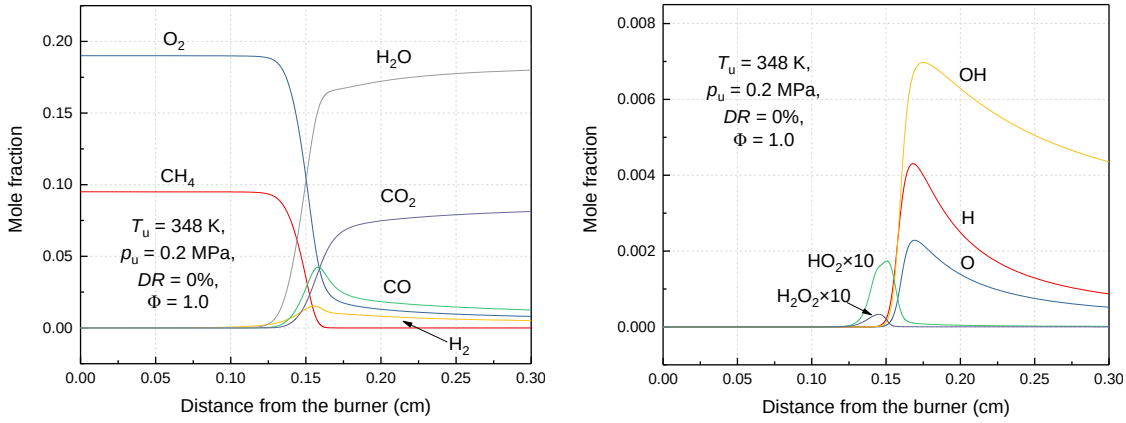

(**b**)

Figure 9. *Cont*.

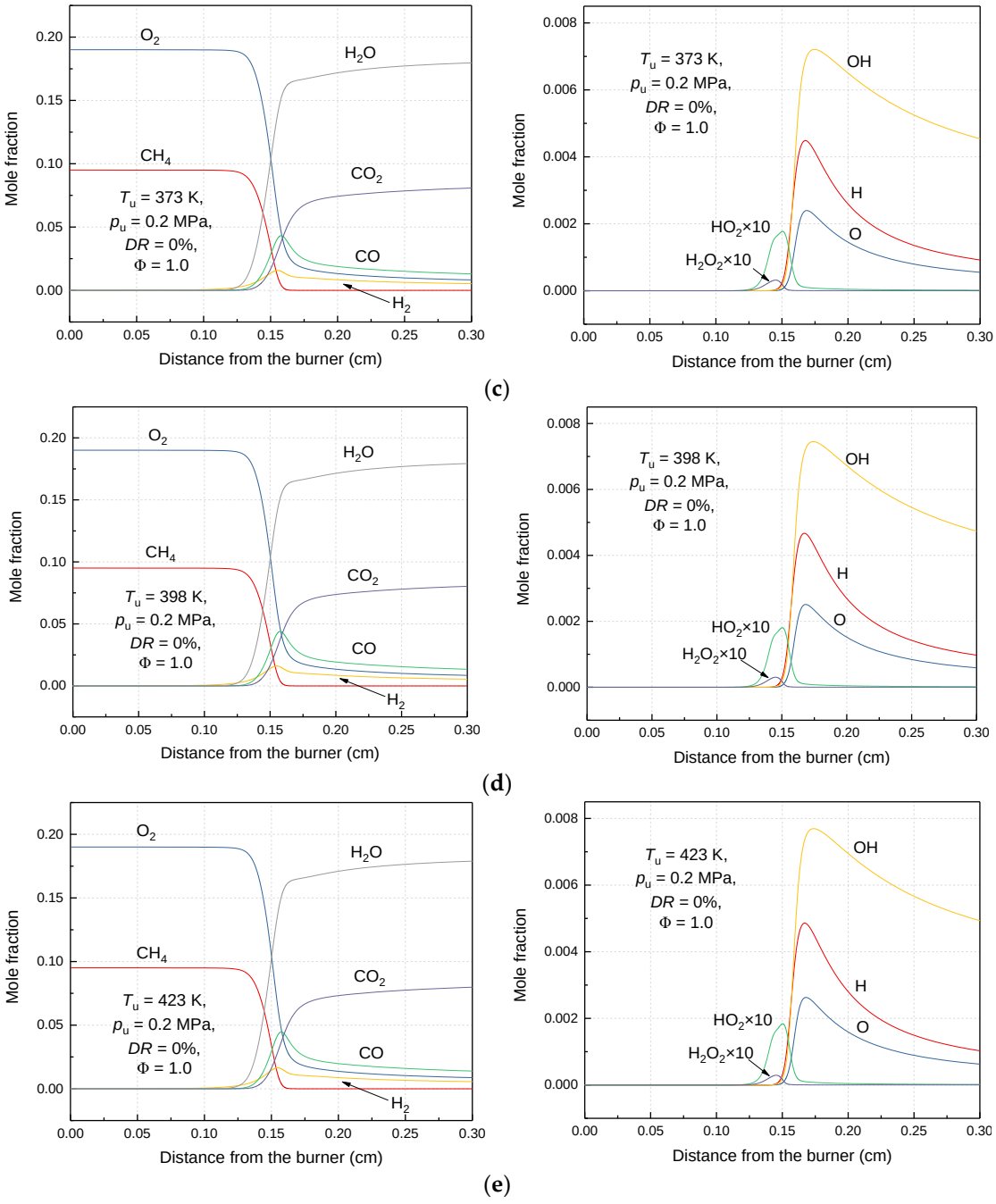

Figure 9. Flame structures under different initial temperatures. (**a**) p_u = 0.2 MPa, T_u = 323 K, *DR* = 0%, Φ = 1.0; (**b**) p_u = 0.2 MPa, T_u = 348 K, *DR* = 0%, Φ = 1.0; (**c**) p_u = 0.2 MPa, T_u = 373 K, *DR* = 0%, Φ = 1.0; (**d**) p_u = 0.2 MPa, T_u = 398 K, *DR* = 0%, Φ = 1.0; (**e**) p_u = 0.2 MPa, T_u = 423 K, *DR* = 0%, Φ = 1.0.

From Figure 10, for the reactants and products, with the increase in the fraction of CO_2, both CH_4 and O_2 decrease, and O_2 decreases more significantly than CH_4. So it can be speculated that decrease in concentration of O_2 can mainly decrease burning velocity. Besides, the final fraction of H_2O and H_2 decrease slightly due to the decrease in CH_4 (the source of H). The maximum fraction of CO decreases slightly due to the suppression on reactions. With the increase in fraction of CO_2, an expansion in range of reaction zone occurs, from the range of 0.1–0.2 cm to 0.075–0.25 cm. For the radicals, it is clear that all the concentrations decrease dramatically except H_2O_2 as it accounts for a really small fraction. OH experiences the most significant decrease, followed by H. It can be concluded that diluent gas can suppress the combustion through decreasing the concentrations of active radicals.

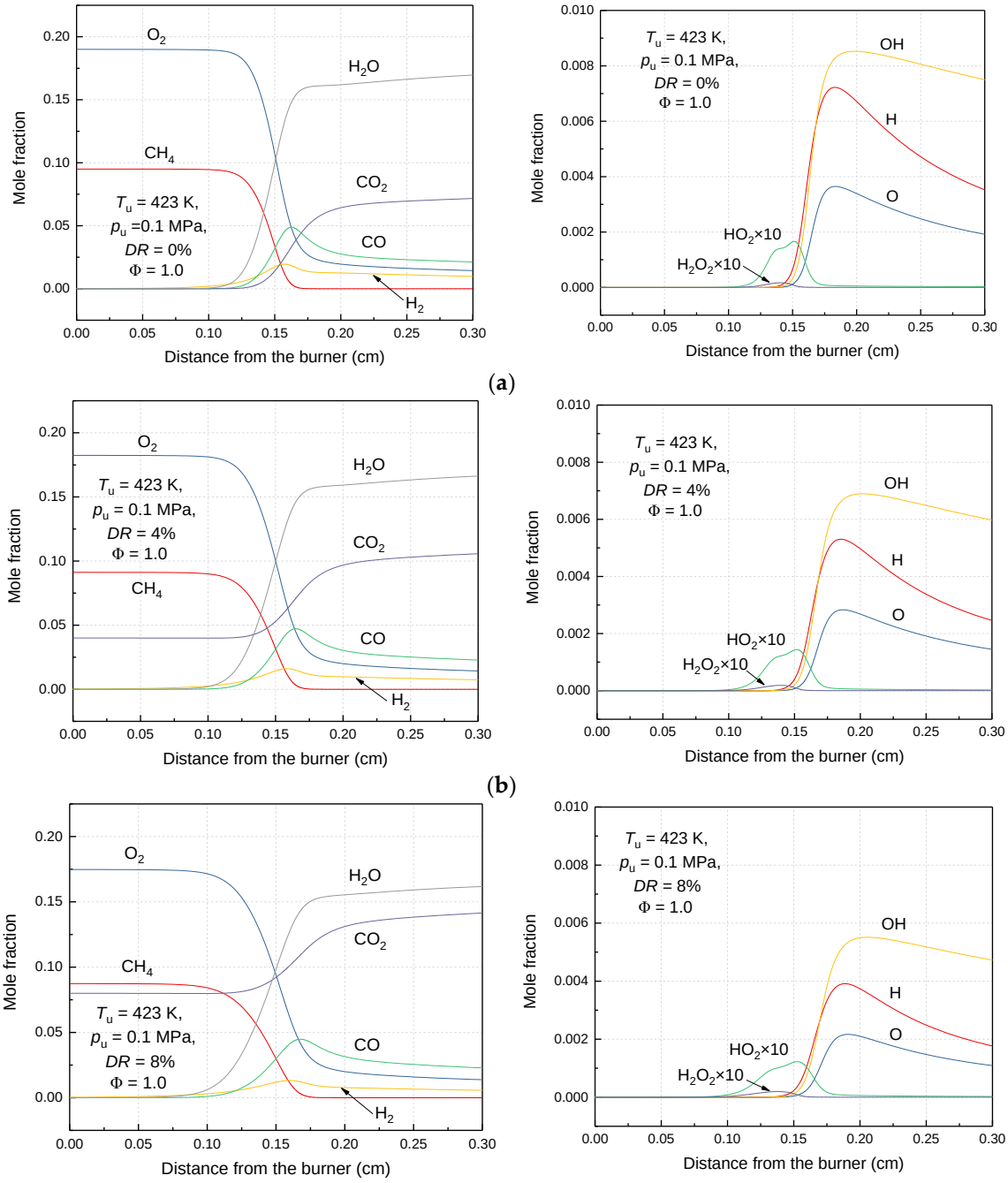

Figure 10. *Cont*.

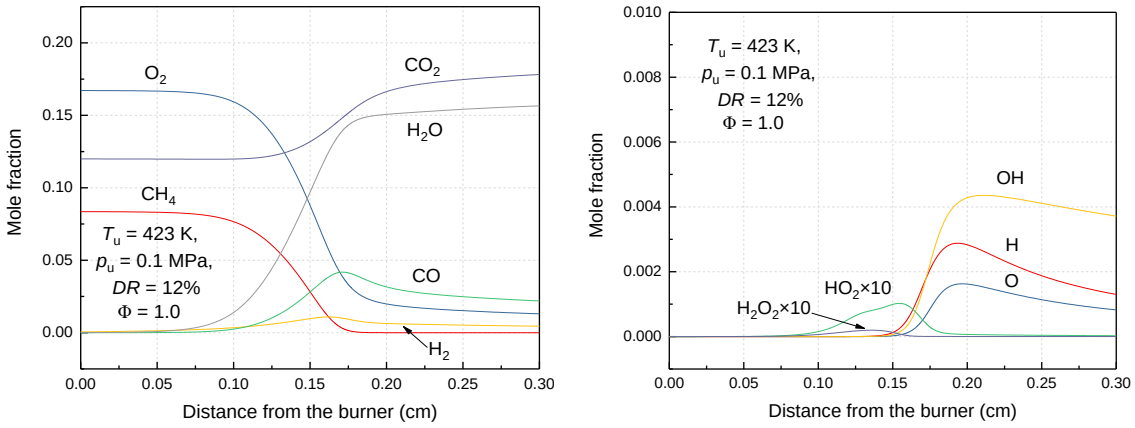

(**d**)

Figure 10. Flame structures under different dilution rates. (**a**) *DR* = 0%, Φ = 1.0; (**b**) *DR* = 4%, Φ = 1.0; (**c**) *DR* = 8%, Φ = 1.0; (**d**) *DR* = 12%, Φ = 1.0.

4.2.2. Concentration of Radicals

From Section 4.2.1, OH, H and O are the most essential active radicals in the combustion of natural gas, and the fraction of OH is the largest among them, followed by H, O accounts for the smallest fraction. In addition, in natural gas-air premixed flame, O mainly comes from the air while H mainly comes from methane. Previous studies proposed that OH and H participate in important elementary reactions [27,28], so this study focuses on the relation between laminar burning velocity and concentrations of OH and H.

Figure 11 illustrates the maximum concentration of H, OH and H + OH under different initial pressures, temperatures and dilution rates, respectively. It is clear that both the maximum concentrations of H and OH increase with initial temperature but decrease with initial pressure and dilution rates. Besides, the maximum fraction of H increases with equivalence ratio monotonously while that of OH rise first and then decreases with the peak value occurs at stoichiometric ratio. The maximum concentration of H + OH shows a similar trend with OH, but the decrease is not as sharp as OH. In addition, it can be seen that the trend of maximum concentration of H + OH is close to that of laminar burning velocity.

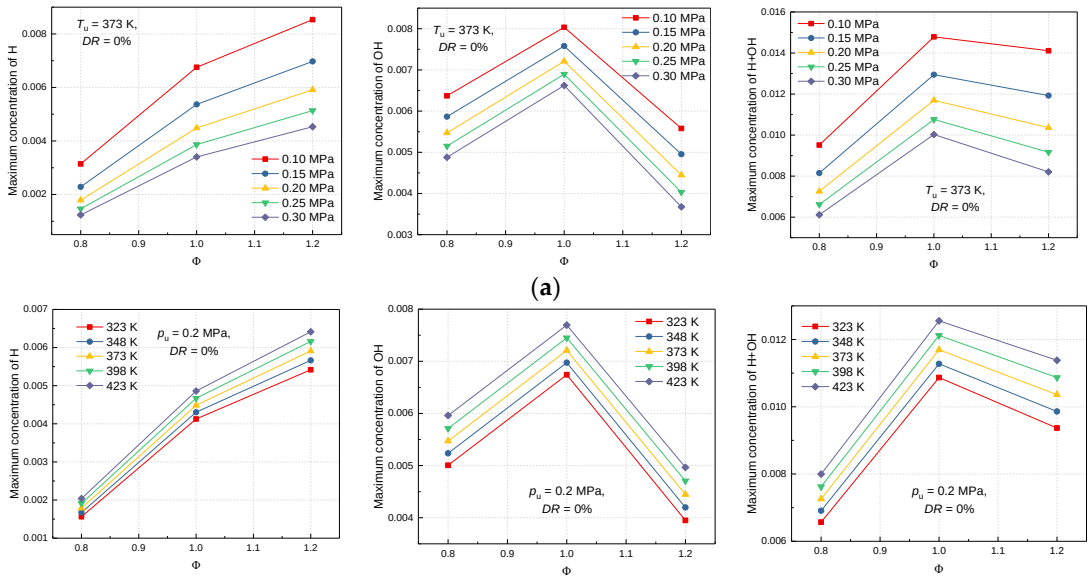

(**b**)

Figure 11. *Cont*.

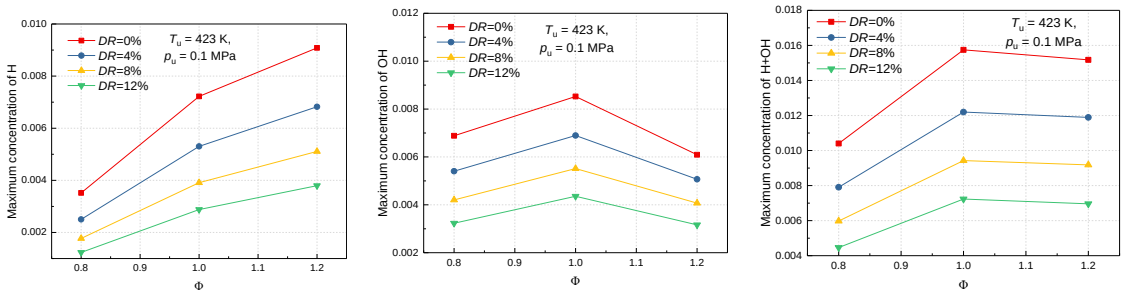

(**c**)

Figure 11. Maximum concentration of H, OH and H + OH. (**a**) Under different initial pressures; (**b**) Under different initial temperatures; (**c**) Under different dilution rates.

To reach a clear understand of the correlation between laminar burning velocity and maximum concentration of H + OH, Figure 12 illustrates the laminar burning velocity (from Chemkin, to avoid the influence of the uncertainty in data from Schlieren) versus maximum concentration of H + OH under different pressures, temperatures and dilution rates with linear fit applied to show the correlation. A simple fitting formula is applied, which is show as Equation (14):

$$u_{\mathrm{L}} = Ac_{\max(\mathrm{O+OH})} + B \tag{14}$$

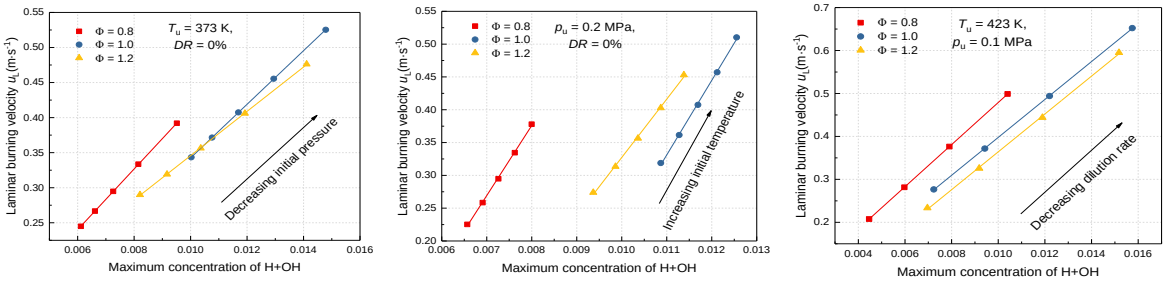

(**a**) (**b**) (**c**)

Figure 12. Laminar burning velocity versus maximum concentration of H + OH. (**a**) Under different initial pressures; (**b**) Under different initial temperatures; (**c**) Under different dilution rates.

The R-square coefficient is used to evaluate the correlation. The larger the R-square is (close to 1), the higher the correlation is. Tables 4–6 show the coefficients (slope, intercept and R-square) of the linear fit to the data of laminar burning velocity versus maximum concentration of H + OH under different initial pressures, temperatures and dilution rates, respectively. The close correlation between laminar burning velocity versus maximum concentration of H + OH can be confirmed under any initial condition as all the R-square values are extremely close to 1. The maximum concentration of H + OH has a high accuracy in predicting burning velocity.

Table 4. Coefficients of the linear fit to the data of laminar burning velocity versus maximum concentration of H + OH under different initial pressures.

T_u = 373 K, DR = 0%	Φ		
	0.8	**1.0**	**1.2**
A	43.27645	38.23116	31.58986
B	−0.01949	−0.0398	0.02985
R^2	0.99998	0.99999	0.99991

Table 5. Coefficients of the linear fit to the data of laminar burning velocity versus maximum mole fraction of H + OH under different initial temperatures.

p_u = 0.2 MPa, DR = 0%	Φ		
	0.8	**1.0**	**1.2**
A	106.77247	113.60037	88.93747
B	−0.47819	−0.91848	−0.56212
R^2	0.99891	0.99897	0.99851

Table 6. Coefficients of the linear fit to the data of laminar burning velocity versus maximum mole fraction of H + OH under different dilution rates.

T_u = 423 K, p_u = 0.1 MPa	Φ		
	0.8	**1.0**	**1.2**
A	49.05268	44.14693	44.08372
B	−0.01146	−0.04367	−0.07669
R^2	1	0.99997	0.99946

5. Conclusions

Based on the initial study of equivalent effect, the effect of initial conditions (initial temperature, initial pressure, dilution ratio and equivalence ratio) on burning characteristics (laminar burning velocity, flame instability, flame structure and concentration of essential radicals) are investigated comprehensively. The main conclusions to prepare for the later equivalent effect study are as follows:

(1) Laminar burning velocity increases with initial temperature but decreases with initial pressure and fraction of CO_2. The intervals in burning velocity among different initial temperature have the highest linearity when comparing with different initial pressure and fractions of CO_2.
(2) Changing initial pressure and temperature do not have significant influence on fractions of reactants and products. Changing fraction of CO_2 can slightly decrease the final concentration of some products.
(3) Fractions of OH, H and O increase with initial temperature but decrease with initial pressure and fraction of CO_2. Laminar burning velocity is highly related to the maximum concentration of H + OH.

Author Contributions: The authors all contributed to the deployment of the paper. Z.H., Z.Z. (Zhennan Zhu) and K.L.; Data curation, Z.Z. (Zhennan Zhu), P.W., Z.Z. (Zinong Zuo) and D.Z.; Formal analysis, Z.Z. (Zhennan Zhu); Funding acquisition, Z.H.; Investigation, Z.Z. (Zhennan Zhu), P.W. and Z.Z. (Zinong Zuo); Methodology, Z.H., Z.Z. (Zhennan Zhu); Project administration, Z.H.; Software, P.W. and Z.Z. (Zinong Zuo); Supervision, Z.H. and K.L.; Writing—original draft, Z.Z. (Zhennan Zhu); Writing—review & editing, Z.H., P.W. and K.L.

Funding: This research was funded by the National Natural Science Foundation of China under Grant No. 51776177, the Foundation of "Chunhui" Plan, Ministry of Education under Grant No. Z2014059.

Acknowledgments: The authors would like to express sincere appreciation to Yunshou Qian, Weilong Sui, Wei Tian and Xueshun Wu for their assistance.

Conflicts of Interest: The authors declare no conflict of interest.

Abbreviations

EGR	exhaust gas recirculation
DAQ	data acquisition
CVC	constant volume chamber
DR	dilution rate
T_u	initial temperature, K
p_u	initial pressure, MPa
Φ	equivalence ratio
λ	thermal conductivity, $W\cdot(m\cdot K)^{-1}$
c_p	specific heat capacity, $J\cdot(kg\cdot K)^{-1}$
D_T	thermal diffusion coefficient, $m^2\cdot s^{-1}$
D_m	mass diffusion coefficient, $m^2\cdot s^{-1}$
Le	Lewis number
ρ_u	density of unburned gas, $kg\cdot m^{-3}$
ρ_b	density of burned gas, $kg\cdot m^{-3}$

R_u	instantaneous flame radius, mm	u_L	laminar burning velocity, m·s^{-1}
S_n	stretched flame propagation speed, m·s^{-1}	σ	thermal expansion ratio
K	stretch rate, s^{-1}	l_f	flame thickness, mm
κ	curvature of spherical flame, mm^{-1}	H	hydrogen radical
S_l	unstretched flame propagation speed, m·s^{-1}	O	oxygen radical
L_b	Markstein length, mm	OH	hydroxide radical

Appendix A

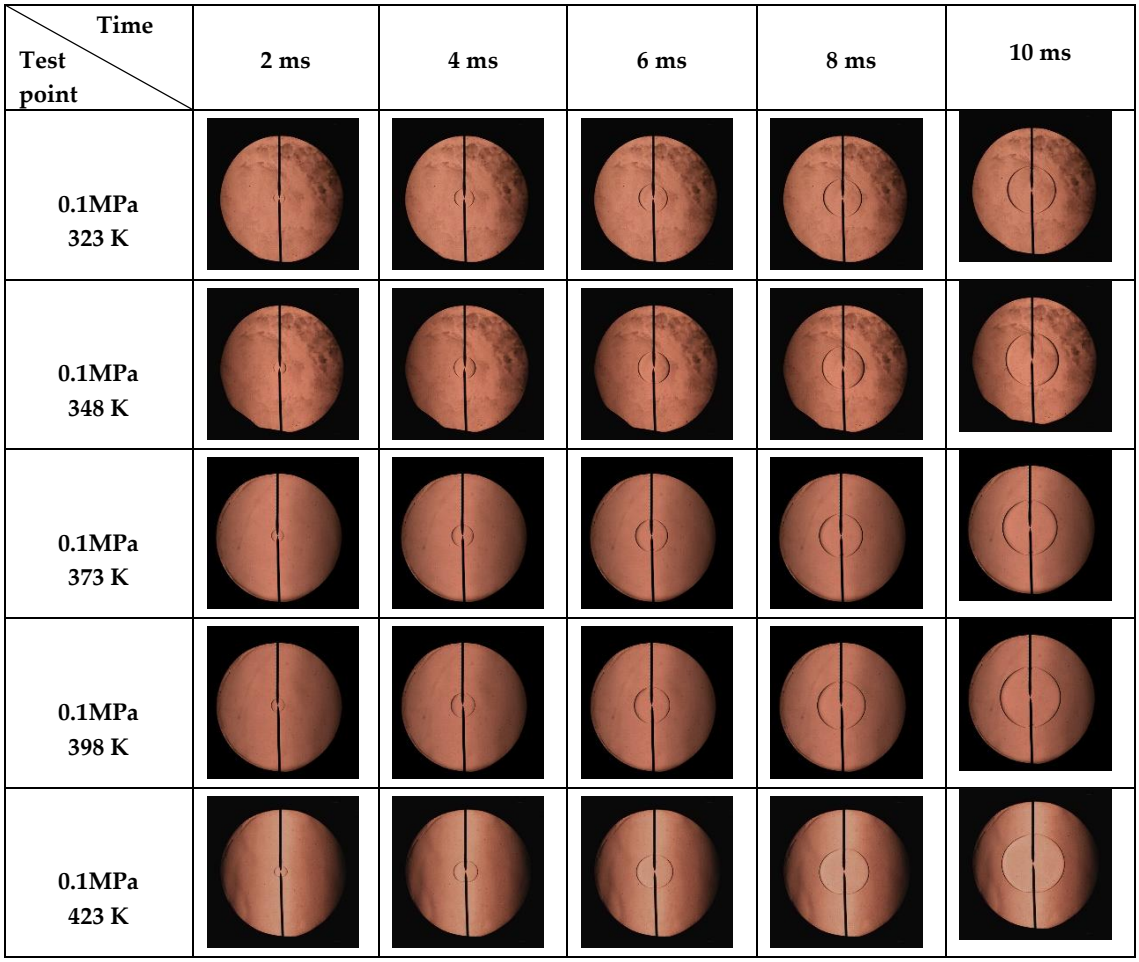

Figure A1. Schlieren photographs of flame propagation under different initial temperatures (*DR* = 2%, Φ = 1.0).

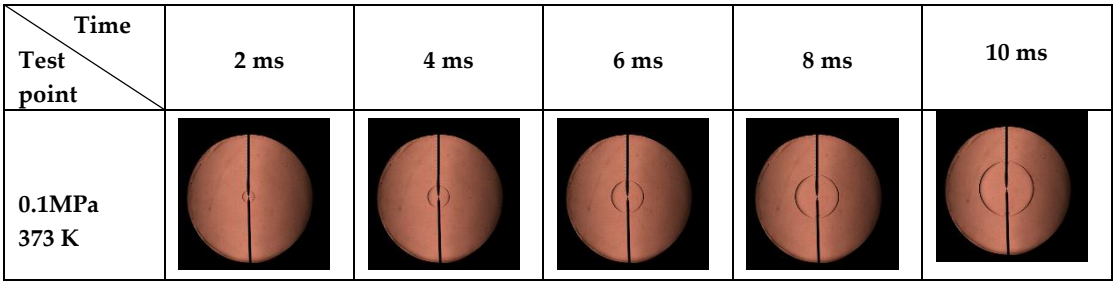

Figure A2. *Cont*.

Time / Test point	2 ms	4 ms	6 ms	8 ms	10 ms
0.1MPa 373 K	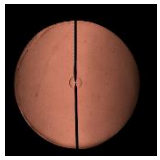	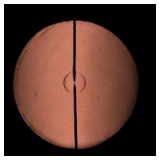	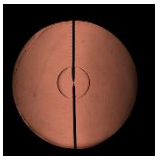	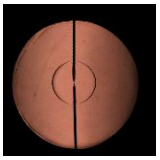	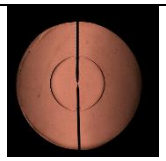

Figure A2. Schlieren photographs of flame propagation under different initial pressures (*DR* = 2%, Φ = 1.0).

Time / Text point	2 ms	4 ms	6 ms	8 ms	10 ms
***DR*=0%**	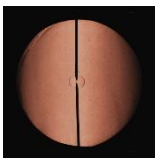	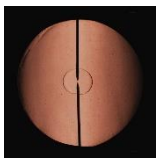	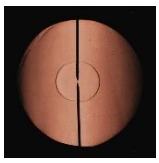	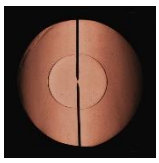	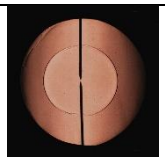
***DR*=4%**	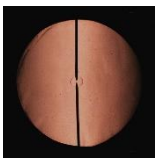	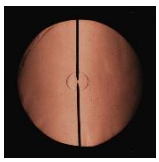	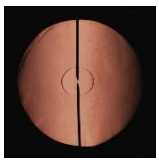	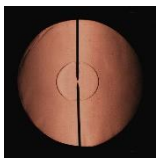	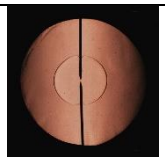
***DR*=8%**	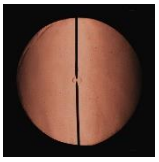	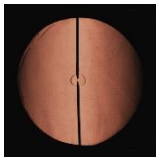	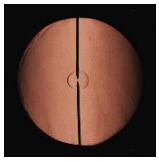	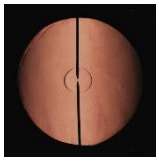	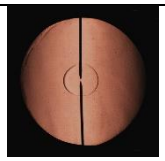
***DR*=12%**	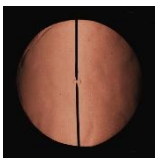	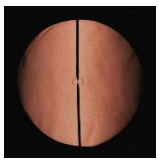	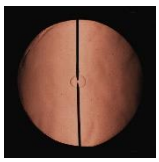	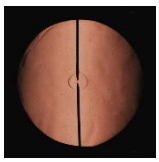	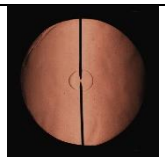

Figure A3. Schlieren photographs for flame propagation process under different dilution rates (T_u = 423 K, p_u = 0.1 MPa, Φ = 1.0).

References

1. Energy Information Administration, US Department of Energy. Available online: https://www.eia.gov/consump-tion/anufacturing/data/2002/index.php/view=methodology/ (accessed on 20 April 2019).
2. Kokjohn, S.; Hanson, P.; Splitter, D. Experiments and modeling of dual-fuel HCCI and PCCI combustion using in-cylinder fuel blending. *SAE Int. J. Engines* **2010**, *2*, 24–39. [CrossRef]
3. Khan, A.R.; Anbusaravanan, S.; Kalathi, L. Investigation of dilution effect with N_2/CO_2 on laminar burning velocity of premixed methane/oxygen mixtures using freely expanding spherical flames. *Fuel* **2017**, *196*, 225–232. [CrossRef]
4. Zhang, Q.; Xu, Z.; Li, M.; Shao, S. Combustion and emissions of a Euro VI heavy-duty natural gas engine using EGR and TWC. *J. Nat. Gas Sci. Eng.* **2016**, *28*, 660–671. [CrossRef]

5. Jahirul, M.I.; Masjuki, H.H.; Saidur, R.; Kalamb, M.A.; Jayedb, M.H.; Wazedcd, M.A. Comparative engine performance and emission analysis of CNG and gasoline in a retrofitted car engine. *Appl. Therm. Eng.* **2010**, *30*, 2219–2226. [CrossRef]
6. Pipitone, E.; Genchi, G. NOx reduction and efficiency improvements by means of the Double Fuel HCCI combustion of Natural Gas-Gasoline Mixtures. *Appl. Therm. Eng.* **2016**, *102*, 1001–1010. [CrossRef]
7. Verma, G.; Prasad, R.K.; Agarwal, R.A. Experimental investigations of combustion, performance and emission characteristics of a hydrogen enriched natural gas fuelled prototype spark ignition engine. *Fuel* **2016**, *178*, 209–217. [CrossRef]
8. Li, W.; Liu, Z.; Wang, Z.; Yun, X. Experimental investigation of the thermal and diluent effects of EGR components on combustion and NOx emissions of a turbocharged natural gas SI engine. *Energy Convers. Manag.* **2014**, *88*, 1041–1050. [CrossRef]
9. Huzayyin, A.S.; Moneib, H.A.; Shehatta, M.S.; Attiaa, A.M.A. Laminar burning velocity and explosion index of LPG-air and propane-air mixtures. *Fuel* **2007**, *87*, 39–57. [CrossRef]
10. Aung, K.T.; Hassan, M.I.; Faeth, G.M. Flame stretch interactions of laminar premixed hydrogen/air flames at normal temperature and pressure. *Combust. Flame* **1997**, *109*, 1–24. [CrossRef]
11. Glassman, I. *Combustion*; Academic Press: New York, NY, USA, 1987.
12. Turns, S.R. *An Introduction to Combustion: Concepts and Applications*; McGraw-Hill Inc.: Singapore, 2000.
13. Zeng, W.; Ma, H.; Liang, Y.; Huc, E. Experimental and modeling study on effects of N_2 and CO_2 on ignition characteristics of methane/air mixture. *J. Adv. Res.* **2015**, *6*, 189–201. [CrossRef]
14. Hu, X.; Yu, Q.; Liu, J. Chemical effect of CO_2 on the laminar flame speeds of oxy-methane mixtures in the condition of various equivalence ratios and oxygen concentrations. *Int. J. Hydrog. Energy* **2016**, *41*, 15068–15077. [CrossRef]
15. Zhang, X.; Huang, Z.; Zhang, Z.; Zheng, J.; Wu, Y.; Jiang, D. Measurements of laminar burning velocities and flame stability analysis for dissociated methanol-air-diluent mixtures at elevated temperatures and pressures. *Int. J. Hydrog. Energy* **2009**, *34*, 4862–4875. [CrossRef]
16. Miao, H.; Jiao, Q.; Huang, Z. Effect of diluent gas on laminar burning velocity of premixed hydrogen enriched natural gas and air mixtures. *J. Combust. Sci. Technol.* **2010**, *16*, 104–110.
17. Huang, Z.; Zhang, Y.; Zeng, K. Measurements of laminar burning velocities for natural gas-hydrogen-air mixtures. *J. Combust. Flame* **2006**, *146*, 301–302. [CrossRef]
18. Markstein, G.H. Experimental and theoretical studies of flame-front stability. *Dyn. Curved Fronts* **1988**, *18*, 413–423.
19. Kelley, A.P.; Law, C.K. Nonlinear effects in the extraction of laminar flame speeds from expanding spherical flames. *Combust. Flame* **2009**, *156*, 1844–1851. [CrossRef]
20. Chen, Z. On the extraction of laminar flame speed and Markstein length from outwardly propagating spherical flames. *Combust. Flame* **2011**, *158*, 291–300. [CrossRef]
21. Zuo, Z.; Pei, Y.; Qin, J.; Xu, H.; Lu, L. Laminar burning characteristics of premixed methane-dissociated methanol-air mixtures under lean burn conditions. *Appl. Therm. Eng.* **2018**, *140*, 304–312. [CrossRef]
22. Cai, X.; Wang, J.; Zhang, W.; Xie, Y.; Zhang, M.; Huang, Z. Effects of oxygen enrichment on laminar burning velocities and Markstein lengths of $CH_4/O_2/N_2$ flames at elevated pressures. *Fuel* **2016**, *184*, 466–473. [CrossRef]
23. Lowry, W.; Vries, J.; Krejci, M.; Petersen, E.; Serinyel, Z.; Metcalfe, W.; Curran, H.; Laminar, G.B. Speed measurements and modeling of pure alkanes and alkane blends at elevated pressures. *J. Eng. Gas Turbines Power* **2011**, *133*, 855–873. [CrossRef]
24. Gas Research Institute. Available online: http://combustion.berkeley.edu/gri-mech/ (accessed on 26 July 2019).
25. Hinton, N.; Stone, R. Laminar burning velocity measurements of methane and carbon dioxide mixtures (biogas) over wide ranging temperatures and pressures. *Fuel* **2014**, *116*, 743–750. [CrossRef]
26. Xu, H.; Liu, F.; Sun, S.; Meng, S.; Zhao, Y. A systematic numerical study of the laminar burning velocity of iso-octane/syngas/air mixtures. *Chem. Eng. Sci.* **2018**, *195*, 598–608. [CrossRef]

27. Hu, E. *Study On Engine and Premixed Laminar Combustion Fueled with Natural Gas-Hydrogen Blends Combined with EGR*; Xi'an Jiaotong University: Xi'an, China, 2010.
28. Butler, C.J.; Hayurst, A.N. Measurements of the concentrations of free hydrogen atoms in flames from observations of ions: Correlation of burning velocities with concentrations of free hydrogen atoms. *Combust. Flame* **1998**, *115*, 241–252. [CrossRef]